

DEVELOPMENT OF KAGRA PHOTON
CALIBRATOR FOR HARDWARE INJECTION
TEST

YU-KUANG CHU



RECOMMENDED FOR ACCEPTANCE

BY THE DEPARTMENT OF

PHYSICS

ADVISER: WO-LUNG LEE

JUNE 2018

Abstract

Photon calibrator (Pcal) is an independent device that can provide artificial input to an interferometric gravitational-wave detector by exerting the radiation pressure of its own laser on the test mass mirror in the interferometer. It not only can provide a fiducial length reference for calibration purpose but also can inject simulated gravitational waveforms to verify the response of the interferometer to the astrophysical gravitational waves, known as hardware injection test. Currently, the injection signals (Excitations) are produced by KAGRA Digital System(DGS). These signals change the intensity of PCal Laser by acousto-optic modulators (AOM) inside the transmitter module of PCal. However, if the output signal from the Digital System is noisy, it force AOM to modulate laser intensity according to such noisy control signal, resulting in noisy radiation force on the End Test Mirror (ETM). In this dissertation, we implemented and characterized an analog filter known as the *De-Whitening filter*. We installed it between Digital System output and PCal to address the noise problem while keeping the accuracy of injected signals.

Acknowledgements

Fist of all, I would like to thank Prof. Takayuki Tomaru and Prof. Nobuyuki Kanda. They support my research activity in Japan not only scientifically but also financially. With their help, I can fully concentrate on my study without worrying about other things. Besides, Dr. Yuki Inoue, Dr. Takaaki Yokozawa, and Dr. Takahiro Yamamoto teach me many practical skills and knowledge during my experiments from the hardware side to the software side. Without their help, it is impossible to get results in this dissertation.

Also, in the last few months, Dr. Chihiro Kozakai and Dr. Darkhan Tuyenbayev joined our calibration group. They helped me a lot to dealing with our X-end PCal and perform the measurement with that.

In addition, people in KEK and KAGRA site help me a lot to manage my stay in Japan and help me to go to the site. They are Emiko Kotaki, Ayako Hagiwara, Ayako Ueda, Mihoko Okinaka, Rie Kikuchi, Dr. Takafumi Ushiba, Koki Okutomi, Takahiro Miyamoto and Yutaro Enomoto.

I also want to thank people in KEK cryogenic lab, including Tomohiro Yamada, Takaharu Shishido, Rishabh Bajpai, and, especially, Bin-Hua Hsieh and Kunihiko Hasegawa. Their practical and mental support made my research life indelible.

I want to thank Dr. Sheau-Shi Pan who teach me how to perform experiments with optics from scratch in ITRI. That is an important experience for me to understand how interferometer works.

At the same time, I really appreciate the strong support from Institute of Physics, Academia Sinica, including Prof. Chih-Hsun Lin and Prof. Ming-Lee Chu, who teach me how to make the De-Whitening Filter circuit design. Discussion with them was critical to make this filter become true. Besides, Pei-Rong Tsai, Tracy Liu and Chia-Yi Lee helped me a lot for managing many administrative questions.

I would like to thank Prof. Rick Savage. He is almost the people who brought me into this field. Even within very limited time, his perception, perseverance, and passion deeply moved me.

Finally and most importantly, I gratefully thank my advisors Prof. Sadakazu Haino and Prof. Wolung Lee. They encourage me to have a chance working on hardware development, which I have never thought before but resulting an incredibly useful experience. Their continuous support in any aspect since the first time we met until now fulfill my master course study.

To my parents.

Contents

Abstract	ii
Acknowledgements	iii
List of Tables	viii
List of Figures	ix
1 Introduction	1
1.1 Introduction to Gravitational Waves	2
1.1.1 What are gravitational waves	2
1.1.2 How to describe gravitational wave	3
1.2 Detection and Reconstruction of Gravitational Wave Signals	5
1.3 Photon Calibrator (Pcal)	7
1.3.1 Principle of Photon Calibrator	7
1.3.2 Evolution of Photon Calibrators	10
2 Hardware Injection through Photon Calibrator	13
2.1 Principle	13
2.2 Experimental Setup	15
3 Signal Generating System	16
3.1 KAGRA Digital Control System	16
3.2 Noise Problem of Injection Signal	19
3.2.1 Noise Sources from Control Signal	20

4 Noise Reduction through De-Whitening Filter	22
4.1 Concept of De-Whitening Filter	22
4.2 Circuit Design	23
4.3 Fidelity of Injection Signals	26
4.4 Noise Reduction Performance	28
4.4.1 Noise Measurement without PCal System	30
4.4.2 Noise Measurement with PCal System	34
5 Validation of Injection Channel	37
6 Discussion and Future Works	41
Bibliography	43

List of Tables

4.1	Acronym of devices in noise measurement plots	29
5.1	Explanation of legends in the injection result	39

List of Figures

1.1	Schematic Diagram of KAGRA Photon Calibrator	7
1.2	Photos of Y-END KAGRA Photon Calibrator	11
1.3	KAGRA Photon Calibrator	12
2.1	Controlling PCal with Digital Control System	15
3.1	The schematic shows the inside of the KAGRA digital system block in Fig. (2.1)	17
3.2	An example schematic of a Digital System Rack	18
3.3	Injection Channel Noise Requirement	19
4.1	De-Whitening filter transfer function	23
4.2	De-Whitening filter circuit	25
4.3	De-Whitening filter board	26
4.4	Transfer function of De-Whitening Filter with Digital Inverse Filter .	27
4.5	Noise Measurement Setup	28
4.6	Noise Measurement Setup	28
4.7	De-Whitening filter noise with short cable	30
4.8	De-Whitening filter noise with long cable	31
4.9	De-Whitening filter noise with different cable length	32
4.10	Noise measurement when the De-Whitening filter is installed at different location	33

4.11	Noise measurement with PCal	34
4.12	Noise measurement with PCal and different location of the De-whitening	35
4.13	Noise measurement with PCal and different power source	36
5.1	Injected Binary Blackhole Merger Signals	40
6.1	Maximum Injection Capability	41

Chapter 1

Introduction

When you got a new camera, you probably will take a lot of testing photos before you start to use it seriously. Similarly, we would like to test our gravitational wave detector before we use it to see the Universe.

Hardware injection test is a process to verify the performance of the interferometer by sending sample signals into the interferometer[1]. Ideally, we should prepare some real gravitational waves as test signals. But it is practically hard to generate large enough artificial gravitational waves that are detectable by current technology.

Therefore, instead of generating gravitational waves, people mimic the effect of celestial gravitational waves by displacing the mirror according to the simulated gravitational waveforms. By comparing the optical readout in the main interferometer with injected signal we can check the response of our interferometer.

Among different ways to push those Test Mass Mirrors in the main interferometer, radiation pressure of external laser beams have been used because of its simplicity and stability. A dedicated auxiliary laser system called Photon Calibrator(PCal) has been developed for this purpose.

In Kamioka Gravitational Wave Detector (KAGRA), in order to get better performance in high frequency regime, we are developing a new PCal with high power

(20 W) laser for our KAGRA detector. Due to the higher power laser, the noise of control signal generated by current control system become a potential problem when we consider the design sensitivity of KAGRA.

In this dissertation, I will briefly explain what is Photon Calibrator and how it works for calibration and hardware injection purposes. Then, I will discuss the noise problem from current signal generating system that is used to control PCal Laser intensity. Finally, we provide a possible solution, the *Analog De-Whitening Filter*, which has been manufactured and tested with a Photon Calibrator in KAGRA, to address the noise problem.

1.1 Introduction to Gravitational Waves

1.1.1 What are gravitational waves

In the General Theory of Relativity proposed by Albert Einstein in 1915, phenomena caused by gravity can be interpreted as results of curved spacetime. This is one of his important works after his ‘Happiest Thought’, which was recorded in his unpublished article “Fundamental Ideas and Methods of the Theory of Relativity, Presented in Their Development”[2]. Among different ways to curve our spacetime, which can be described by corresponding metric tensor fields, there exist wavelike solutions describing ripples of spacetime known as gravitational waves.

However, the physical reality of gravitational waves was not so clear to everyone in the early days, even to Einstein himself [3, 4]. The main problem is that there exist some gauge degree of freedom in the theory due to the arbitrariness of coordinate choices. We have to know whether the gravitational waves we found are just gauge waves (vibration of coordinates) or the wave can have some observable consequences.

One of the most important observational evidence implying the existence of real gravitational waves is the Hulse-Taylor pulsar [5]. Taylor demonstrated that the

change of pulsar rotation speed can be explained by emission of gravitational wave [6, 7].

Finally, on September 14th, 2015, the first direct detection of gravitational wave signal [8] is done by Laser Interferometer Gravitational-Wave Observatory(LIGO) detectors in the United States.

1.1.2 How to describe gravitational wave

In Einstein's General Relativity, gravitational effects are realized by geometry of spacetime. According to a great mathematician Bernhard Riemann, we can describe the geometry of certain space by telling the "distance" between nearby points in the space. Practically, the information of distance between nearby spacetime points form a tensor called metric, which means the measure of distance. By choosing a coordinate system, one can write down those corresponding components of a metric tensor g .

$$g_{\mu\nu} = \begin{pmatrix} g_{00} & g_{01} & g_{02} & g_{03} \\ g_{10} & g_{11} & g_{12} & g_{13} \\ g_{20} & g_{21} & g_{22} & g_{23} \\ g_{30} & g_{31} & g_{32} & g_{33} \end{pmatrix} \quad (1.1)$$

Now, we can calculate spacetime distance ds between two nearby points by their coordinate separation:

$$ds^2 = g_{\mu\nu}dx^\mu dx^\nu \quad (1.2)$$

Through the interaction between matter and spacetime, matter can curve our Universe. The whole story can be resolved by solving Einstein equation,

$$R_{\mu\nu} - \frac{1}{2}g_{\mu\nu}R = \frac{8\pi G}{c^4}T_{\mu\nu} \quad (1.3)$$

which is a non-linear differential equation of metric tensor field $g_{\mu\nu}(x^\alpha)$ since the Ricci tensor $R_{\mu\nu}$ contains the metric tensor and its differential. To understand the “shape” of our spacetime described by Eq. (1.2), one can get the metric tensor field in it by solving the Eq. (1.3) with a given matter filed $T_{\mu\nu}$, a gauge choice, and some boundary conditions.

Furthermore, it is similar to the case in Electrodynamics, in which we can have electromagnetic waves solutions by solving Maxwell equations, that we can have gravitation wave solutions by solving Einstein equation. The situation will become more clear if we linearize the Einstein equation and choose coordinate or gauge properly.

A wave equation derived from a linearized Einstein equation can be expressed in the following way

$$\square \bar{h}_{\mu\nu} = -\frac{16\pi G}{c^4} T_{\mu\nu} \quad (1.4)$$

Where $\bar{h}_{\mu\nu} = h_{\mu\nu} - \frac{1}{2}\eta_{\mu\nu}$ is the trace-reversed metric perturbation on flat spacetime background. Near the gravitational wave detector, where $T_{\mu\nu}$ is practically small enough to be ignore, one can simplify Eq. (1.4) to be:

$$\square \bar{h}_{\mu\nu} = 0 \quad (1.5)$$

Then, a conventional coordinate choice known as transverse-traceless (TT) gauge, where the coordinate themselves are attached to a set of free falling test masses, can make the calculation even simple. In this case, the propagating gravitational wave along z -direction in a local “Cartesian” coordinate can be described by corresponding metric components $h_{\mu\nu}$:

$$h_{\mu\nu}^{TT}(t, z) = \begin{pmatrix} 0 & 0 & 0 & 0 \\ 0 & h_+(ct - z) & h_x(ct - z) & 0 \\ 0 & h_x(ct - z) & h_+(ct - z) & 0 \\ 0 & 0 & 0 & 0 \end{pmatrix} \quad (1.6)$$

Gravitational wave detectors are build to measure these spacetime distance perturbation, i.e. the contraction of $h_{\mu\nu}^{TT}(t, z)$ and coordinate separations dx^μ according to Eq. (1.2) integrated over the “size” of the detector. For more detail calculation, one may refer to some related textbooks, e.g. [9].

1.2 Detection and Reconstruction of Gravitational Wave Signals

The interaction of a detector and gravitational waves can have different interpretation due to different coordinate choices [10]. It is quite similar to that the magnetic force in one observational frame may be electric force in the other frame. Of course, the physical consequence should be coordinate independent. Therefore, we are not going to worry about this issue too much in the following context.

Practically, in order to detect tiny GW signals. A dual recycled Michelson interferometer with Fabry-Pérot arm cavities has been the standard setup of current ground-based gravitational wave detectors. The response, or the sensing function $C(f)$, of such detector to the incoming gravitational wave signal can be approximately described by following expression, which is the Eq.(6) in [11]:

$$C(f) = \frac{g e^{-2\pi i f L/c} \times (1 + if/z)}{1 + if/|p|Q_p - f^2/|p|^2 - \xi^2/f^2} \quad (1.7)$$

where the g is the optical gain and the $e^{-2\pi ifL/c}$ is the delay caused by signal propagation in arms. Besides, a coupled-cavity pole with some shift caused by signal recycling cavity can be described by two real parameters, $|p|$ and Q_p . Finally, the ξ^2 accounts for optical spring effect, and the homodyne zero z can be derived from homodyne detection angle and some parameters [11]. One way to get the $h(t)$ is to apply the inverse sensing function $C^{-1}(f)$ to the detected optical readout.

In a real detector, these parameters may vary with time. Therefore, in order to reconstruct the gravitational wave signal, $h(t)$, from the sensed optical readout accurately, tracking the time dependency of these parameters is an indispensable work [12, 13].

To track variations of these parameters, one can change the length difference between X-arm and Y-arm of the interferometer with known displacement at several frequencies by injecting calibration lines, which are sinusoidal test signals with known amplitudes that are displacing test-mass-mirrors in detectors, and compares the observed calibration line amplitude in the optical readout with the injected calibration line strength, thereby solving the detector response at the frequency of the selected calibration line. Then, those parameters that describe the status of interferometer can be calculated [13].

In order to prepare these calibration lines, a Photon Calibrator (PCal), which is a device independent from the main interferometer control loop, has been developed to generate high accuracy displacement of the end-test-mirrors. Details are given in the next section.

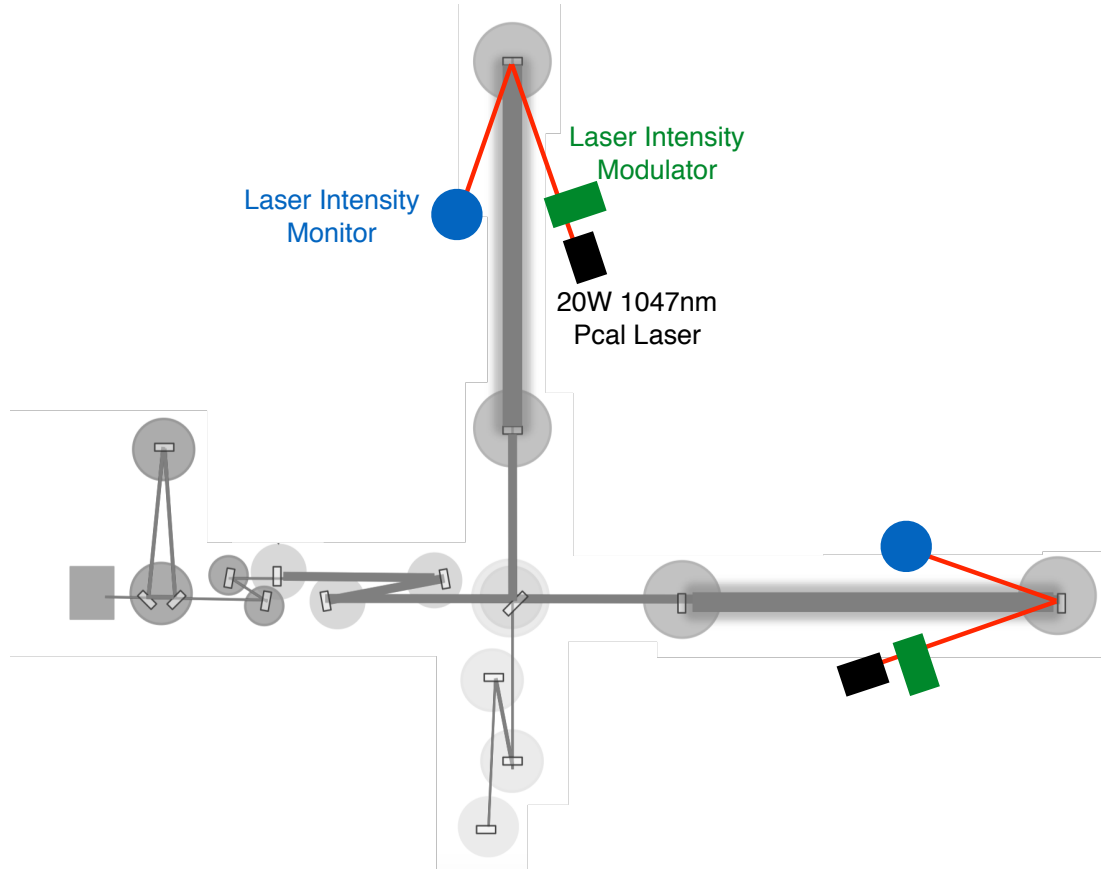


Figure 1.1: Schematic Diagram of KAGRA Photon Calibrator. Two sets of Photon Calibrators have been installed in front of ETMX (X-arm End-Tess-Mirror) and ETMY

1.3 Photon Calibrator (Pcal)

1.3.1 Principle of Photon Calibrator

Photon Calibrator is an auxiliary laser with a high precision intensity modulator. It is installed in front of the End-Test-Mass Mirror(ETM) and can push the ETM with the radiation force from its own Laser beam as depicted in Fig.(1.1). To generate any artificial $h(t)$ by PCal, we have to translate desired $h(t)$ into corresponding force $F(t)$ exerting on ETM. This can be done by using equation of motion of the ETM suspend by its suspension system. Then, we control the Pcal Laser output intensity $P(t)$ such that the radiation force exerted on ETM is $F(t)$ we calculated before.

The radiation force caused by a continuous laser beam can be calculated by its momentum transfer per unit time.

$$\mathbf{F} = \frac{\Delta \mathbf{p}}{\Delta t} \quad (1.8)$$

For our purpose, the laser beam will be almost entirely reflected from ETM. Therefore, the momentum transfer to ETM per unit time should be almost equal to twice of longitudinal momentum flux carried by PCal laser beam.

$$\mathbf{F}_{\text{on ETM}} = \frac{\Delta \mathbf{p}_{\text{ETM}}}{\Delta t} = 2 \cos(\theta) \frac{\Delta p_{\text{Laser}}}{\Delta t} \quad (1.9)$$

where θ is the angle of incident.

Furthermore, one can express the momentum flux of light in terms of its intensity through Eq.(1.13), which can be derived from either classical point of view with its Poynting vector or Quantum Mechanical approaches that we adopt here by dealing with photons.

$$E_\gamma = \hbar\omega \quad (1.10)$$

$$p_\gamma = \hbar k \quad (1.11)$$

$$= \frac{k}{\omega} E_\gamma = \frac{1}{c} E_\gamma \quad (1.12)$$

$$\underbrace{\frac{\Delta p_{\text{photons}}}{\Delta t}}_{\substack{\text{momentum flux due to} \\ \text{photons in a continuous laser beam}}} = \frac{1}{c} \underbrace{\frac{\Delta E_{\text{photons}}}{\Delta t}}_{\substack{\text{Intensity of laser beam} \\ \text{defined as } P}} = \frac{P}{c} \quad (1.13)$$

Combining Eq.(1.9) and Eq.(1.13), the force that PCcal can give ETM is:

$$F_{\text{PCal}}(t) = \frac{2 \cos(\theta)}{c} P(t) \quad (1.14)$$

On the other hand, the equation of motion of suspend ETM with mass M can be modeled as:

$$\ddot{x}(t) + b\dot{x}(t) + \omega_0^2 x(t) = \frac{F(t)}{M} \quad (1.15)$$

where $M\omega_0^2 x(t)$ is the restoring force from suspension system and $Mb\dot{x}(t)$ is the damping force. Both of them are calculated up to leading order since the displacement amplitude and the velocity of ETM are suppose to be small.

The impulse response of Eq.(1.15) is

$$x(t) = \frac{b}{\omega_1} e^{-\frac{b}{2}(t-t_0)} \sin[\omega_1(t-t_0)] \quad (1.16)$$

where $\omega_1 \equiv \sqrt{\omega_0^2 - b^2/4}$ is the resonance frequency of the damped oscillator. When b approaches to zero, i.e. the damping effect becomes smaller, ω_1 will get closer to ω_0 , which is the resonance frequency of the undamped system.

And in frequency domain, we have

$$x(\omega) = \frac{-1}{\omega^2 - \omega_0^2 - i\omega b} \frac{F(\omega)}{M} \quad (1.17)$$

As long as $\omega^2 \gg \omega_0^2$ and $\omega \gg b$, Eq.(1.17) can be approximated as

$$x(\omega) = \frac{-1}{\omega^2} \frac{F(\omega)}{M} \quad (1.18)$$

By substituting the Fourier transformed Eq.(1.14) into Eq.(1.18), we can get the expression of $x(\omega)$ by frequency domain PCal laser intensity modulation $P(\omega)$

$$x(\omega) = \frac{-1}{M\omega^2} \frac{2P(\omega) \cos(\theta)}{c} \quad (1.19)$$

1.3.2 Evolution of Photon Calibrators

The original PCal was proposed by Glasgow group [14] in order to calibrate their 10 meter interferometer prototype. With the PCal, they can displace the mirror of their arm cavity without attaching extra components, e.g. magnets, on the mirror, which might change its mechanical properties like Q-factor resulting unwanted side-effect. In their experiment, they used a single laser beam hitting on the center of ETM and successfully see these sin waves in the the readout of their interferometer.

However, people in LIGO pointed out that since the mirror is not a perfect rigid body, the PCal beam may unintentionally deform the mirror surface when it pushes the mirror [15]. By separating the PCal beam into two beams pointed at some special points, e.g. nodal points of mirror vibration normal modes, the surface deformation can be controlled within an acceptable regime[15]. Accompanied with several upgrades, and studies about the absolute length, or the absolute amplitude of $h(t)$, calibration that requires the knowledge of the absolute power of the PCal leaser beam, a “second generation” PCal has been developed and worked with advanced LIGO detectors [16].

Based on the advanced LIGO PCal design, we are developing new Photon Calibrators for KAGRA. Photos and schematics are shown in Fig. 1.2 and Fig. 1.3 respectively. The most important feature is that we are using a 20W input laser in our PCal, which is ten times stronger than the current LIGO PCal. With higher power laser, the expected maximum displacement capability should be stronger, especially for high frequency signal that suffer more from $1/f^2$ force-to-length tranfer function which is explained in Eq.(1.19) and depicted in Fig. 6.1.

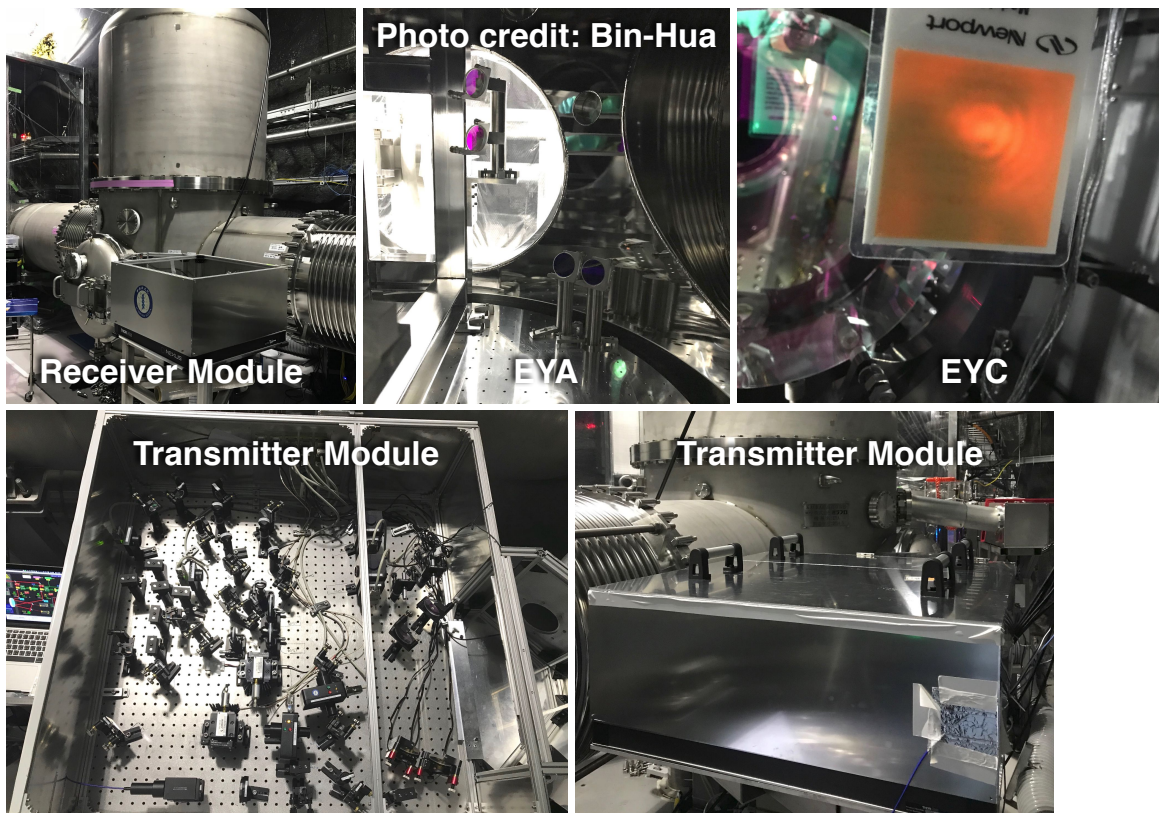


Figure 1.2: Photos of Y-END KAGRA Photon Calibrator

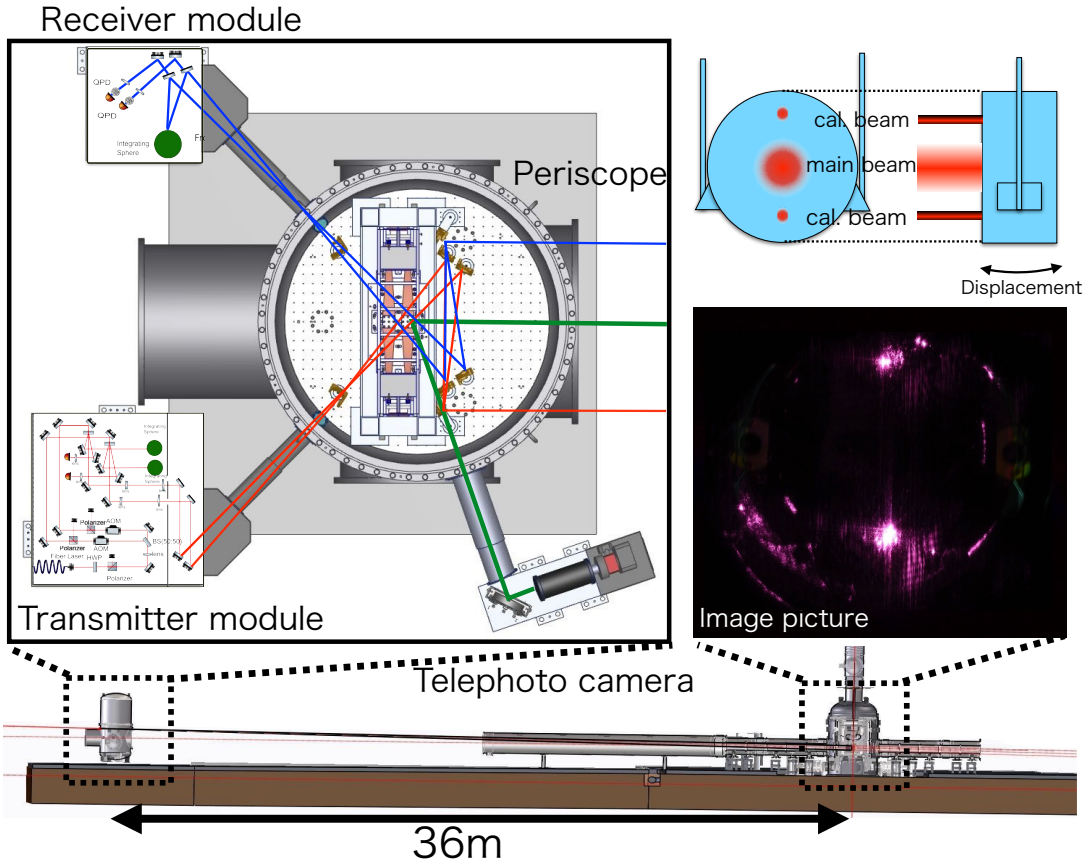


Figure 1.3: KAGRA Photon Calibrator. The KAGRA PCal is comprised of three parts including a transmitter module (Tx), a receiver module (Rx), and a telephoto camera (Tcam). First, the input Ytterbium fiber laser is split into two beams, which will be the upper and lower PCal beams on the ETM. Then, their intensity is modulated by two AOMs with their own feedback control loops known as Optical Follower Servos (OFS). At the same time, an out-of-loop PD equipped with an integrating sphere called TxPD inside the Tx module keep monitoring the intensity of a sampled laser beam from each of the PCal main output beams. Now, the modulated PCal beams from the Tx module will be sent to the ETM, which is 36m far away from the PCal, thereby pushing the ETM by its own radiation pressure. Finally, the intensity and position of reflected beams can be monitored by PDs inside the Rx module. Also, to check the exact position of PCal beam spots on the ETM, we can take photos of them with the Tcam and adjust their positions to the optimal ones.

Chapter 2

Hardware Injection through Photon Calibrator

Hardware inject test is an important way to understand the output form our interferometer. It can help us to check not only the response of our detector like Eq. 1.7, but also the property of detector noise in the presence of incoming gravitational waves [1]. For both purposes, a hardware injection system with high accuracy and low noise is required. In the mean time, Photon Calibrator is an appealing option as a device providing injecting signals.

2.1 Principle

As I described in Sec.1.3.1, we can generate the desired ETM displacement $x(t)$ by changing the PCal laser intensity $P(t)$. One can calculate the corresponding $P(t)$ by performing inverse Fourier transform to Eq.(1.19).

$$\int_{-\infty}^{-\infty} x(\omega) e^{i\omega t} d\omega = \frac{-2 \cos(\theta)}{Mc} \int_{-\infty}^{-\infty} \frac{P(\omega)}{\omega^2} e^{i\omega t} d\omega \quad (2.1)$$

$$\frac{Mc}{-2 \cos(\theta)} \int_{-\infty}^{-\infty} x(\omega) \omega^2 e^{i\omega t} d\omega = P(t) \quad (2.2)$$

where

$$\text{Mass of ETM} \quad M = 23 \text{ kg}$$

$$\text{Angle of Incident} \quad \theta = 0.72 \text{ deg}$$

$$\text{Speed of Light} \quad c = 2.998 \times 10^8 \text{ m/s}$$

Whenever you have your GW waveform template in hand, you can plug them into Eq. (2.2). Then the calculated $P(t)$ will be the signal sent into PCal for PCal laser intensity modulation.

Also, if we have the complete model of ETM suspension, we can substitute the ω^2 factor in Eq.(2.2) by the full displacement-to-force transfer function. This could be important if we are going to inject some low frequency signals.

2.2 Experimental Setup

Once we got the necessary $P(t)$ from the desired $x(t)$ through Eq.(2.2), we can start to modulate our PCal laser intensity according to that $P(t)$. The way how we control our PCal laser intensity is explained in Fig. (2.1).

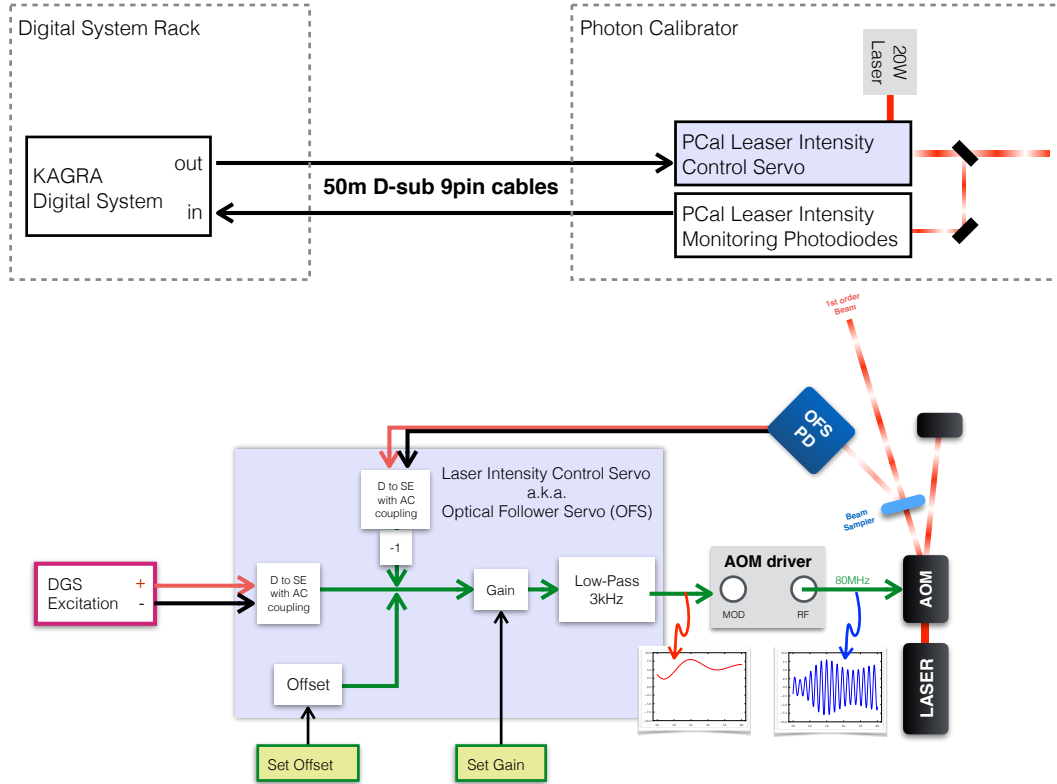


Figure 2.1: Controlling PCal with Digital Control System. The PCal laser beam that will be sent to ETM is the first order diffracted beam of a 20W input laser form an acousto-optic modulator(AOM). Its intensity is controlled by analog control signals generated form our KAGRA Digital System, which has been used as an arbitrary function generator in this case. An analog feedback control loop called Optical Follower Servo(OFS) has been implemented to reduce non-linear response of AOM and laser intensity noise of 20W input laser.

Chapter 3

Signal Generating System

3.1 KAGRA Digital Control System

The Digital Control System used in KAGRA is based on the Advanced LIGO Digital System [17]. In this system, analog control signals can be generated from a Digital-to-Analog Convertor(DAC) installed in any realtime computer known as a Front-End machine located around interferometer. Between the DAC output and experimental device, a customized analog low-pass filter called an Anti-Image filter [18] has been installed for removing unwanted high frequency signal, the Image, due to digitized output from DAC.

Inside a Front-End machine, the signal that will be sent to a DAC are prepared by a realtime software [19], which is generated from several building blocks, realtime models, by a customized parser and compiler [20]. Each realtime model can be running at specifiable sample rate on a dedicated CPU core. However, currently, all DAC cards installed at KAGRA site are 16bit, 64kHz (65536Hz) ones. Therefore, a mandatary model named Input/Output Processor(IOP) model will always run at 64kHz [19], communicating with a DAC card and other "slave" models, in which people can put digital filters, signal generators, etc [21].

On the other hand, the digital system also works as a Data Acquisition System (DAQ). An analog signal coming from a transducer (e.g. a photodiode) can be sampled by an Analog-to-Digital Convertor(ADC). After that, processed by optional digital filters, it could be sent back to an experimental device trough a DAC, be analyzed by an online diagnosis tool, or be stored into a frame file through the frame-builder. To avoid aliasing effect, which is caused by a finite sampling rate, a customized analog low-pass filter, which has the same circuit design as the AI filter, called an Anti-Alias filter [18] has been inserted between the incoming signal and the ADC card.

Unfortunately, the noise performance of such general purpose system do not meet the requirement of KAGRA Photon Calibrator in current setup. The noise coming from the digital system output can be directly translated into the PCal laser intensity noise, which will displace the ETM in a noisy way.

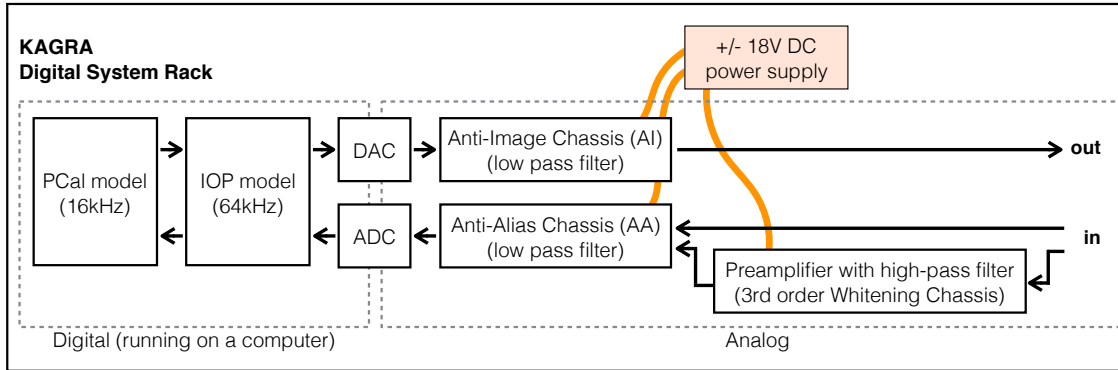


Figure 3.1: The schematic shows the inside of the KAGRA digital system block in Fig. (2.1). A optional whitening chassis is used as a preamplifier that only amplify the signal above 10Hz.

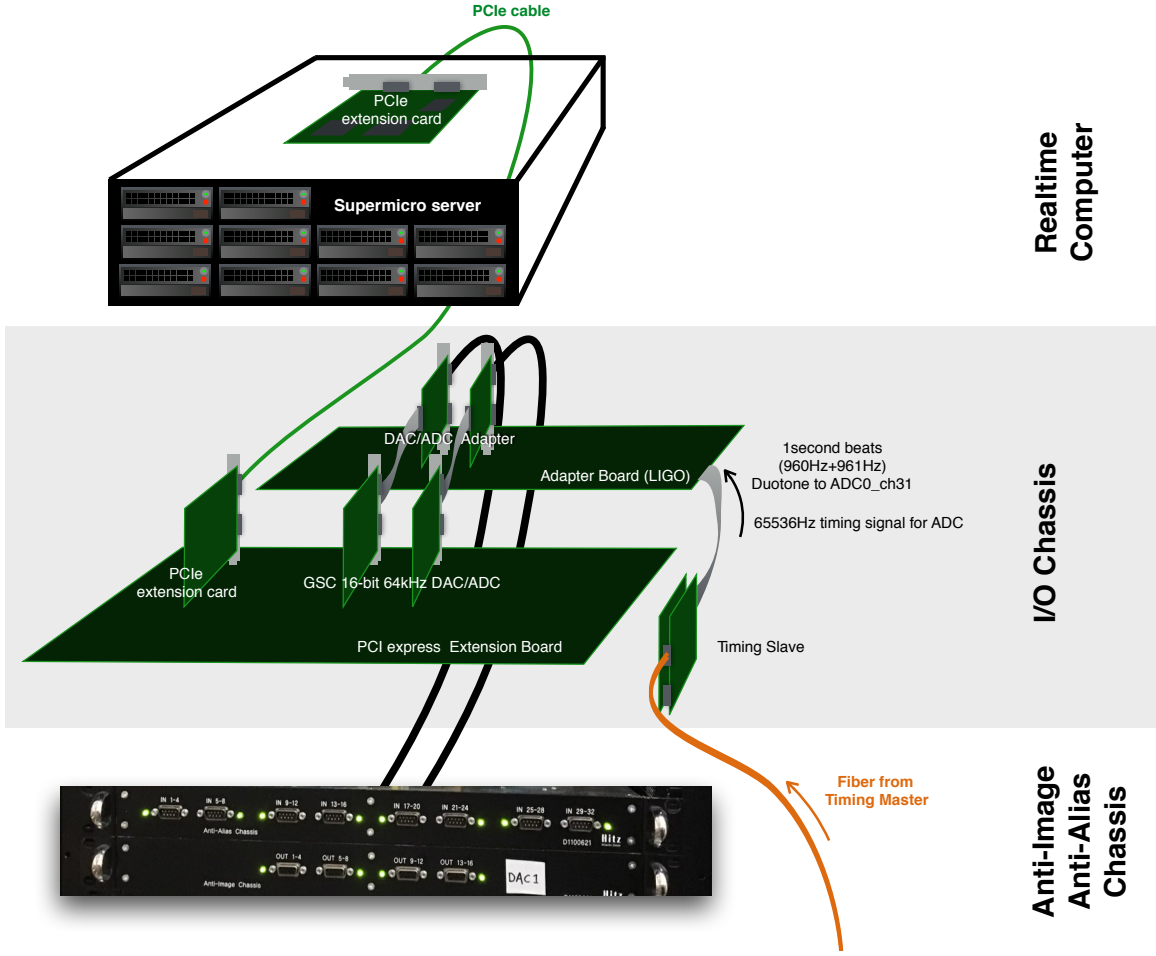


Figure 3.2: An example schematic of a Digital System Rack. As a user of Digital system, you may connect your experimental device to the D-sub 9 pin connectors in the front panel of AA/AI chassis. The conversing between analog and digital signal can be done by ADC and DAC cards inside the I/O chassis. In order to synchronize different ADC/DAC cards located over the whole interferometer, a Time Distribution System (TDS) has been build. It receive the timestamp from a GPS antenna and try to synchronize all Timing Slaves to a central Timing Master. Then, in all I/O chassis, synchronized timing slaves can generate clock signals simultaneously.

3.2 Noise Problem of Injection Signal

The noise contains in the injection signal should not excess the sensitivity curve of the main interferometer. Practically, a 1/10 safety factor has been considered, which means we set our noise requirement as ten times below the KAGRA sensitivity[22]. For the convenience of comparison, we translate the displacement noise requirement into $V/\sqrt{\text{Hz}}$ for electrical excitation signal by considering both the $1/\omega^2$ force-to-length transfer function and the Volt-to-Watt conversion factor that determined by PCal control circuit configuration.

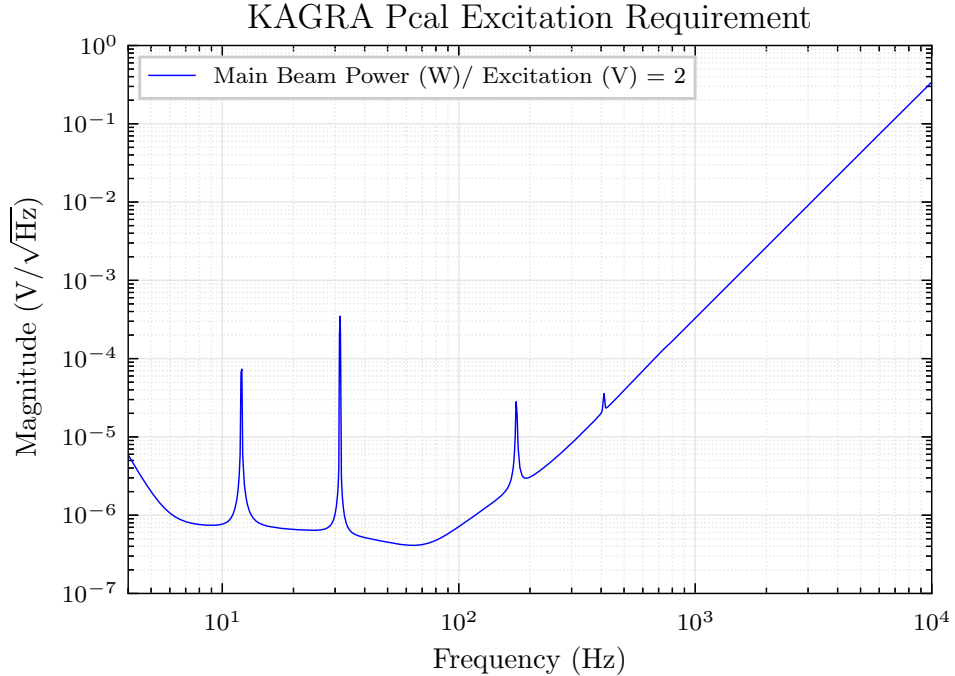


Figure 3.3: Injection Channel Noise Requirement. It is calculated by combining Eq. 1.19 and Eq. 3.2.

$$\Delta L(f) < \frac{1}{10} \times (\text{KAGRA length sensitivity}) \quad (3.1)$$

$$\Delta L(f) = \frac{2\Delta P(f) \cos(\theta)}{c} \frac{1}{M(2\pi f)^2} < \frac{1}{10} \Delta h(f) L \quad (3.2)$$

3.2.1 Noise Sources from Control Signal

Quantization Noise of DAC

The origin of quantization error is coming from the difference between desired analog output and quantized Digital to Analog Converter(DAC) output value. Roughly speaking, it shows up like white noise that is spread from DC to Nyquist frequency, i.e. the half of the sampling frequency $F_s/2$. The Root Mean Square value of quantization noise has the order of voltage difference corresponding to last digit or Least Significant Bit(LSB). In time domain, we can calculate its standard deviation.

$$\sigma_x = \sqrt{\frac{1}{12}\delta x_{LSB}} \quad (3.3)$$

For a 16-bit 64kHz DAC with output range between ± 10 Volts,

$$\sigma_x = \sqrt{\frac{1}{12}\delta x_{LSB}} \quad (3.4)$$

$$= \sqrt{\frac{1}{12} \frac{(10) - (-10)}{2^{16}}} \quad (3.5)$$

$$= 8.81 \times 10^{-5} \text{ Volts} \quad (3.6)$$

In frequency Domain, the quantization noise is distributed from DC to 32768Hz; therefore, we have the amplitude spectral density (ASD):

$$ASD = \sqrt{PSD} \quad (3.7)$$

$$= \sqrt{\frac{\sigma_x^2}{32768}} \quad (3.8)$$

$$= 8.81 \times 10^{-5} \sqrt{\frac{1}{32768}} \quad (3.9)$$

$$= 4.87 \times 10^{-7} \text{ Volts}/\sqrt{\text{Hz}} \quad (3.10)$$

which is a technical limitation of current used signal generating system.

AC Power Lines

The frequency of AC power used in in the KAGRA site is 60 Hz. If the AC power sneak into our signal path, it may create 60Hz and its harmonics in our signal. Also, although most of our devices are supplied by DC power, those DC power are rectified from AC power source. With a full-wave rectification circuit, another series of AC power lines started from 120 Hz could be created. In our De-Whitening filter, we do not put too much effort to reduce AC power lines comparing to other board-band noses. We only adopt the standard LM2941/LM2991 voltage regulation circuit and implement it in the De-Whitening chassis. In the future, we should come back to this issue if necessary.

Chapter 4

Noise Reduction through De-Whitening Filter

4.1 Concept of De-Whitening Filter

Considering a situation in which the Photon Calibrator received white, i.e. frequency independent, excitation signal noise, it will generate $1/f^2$ displacement noise on End-Test-Mirror because the force-to-displacement transfer function contains a $1/f^2$ feature. If we put an analog filter that has frequency response proportional to f^2 between the excitation signal and the PCal excitation input port, we may create colored, f^2 , laser intensity noise from white electrical noise of the excitation signal. Then, such colored noise will be whitened by the $1/f^2$ force-to-displacement transfer function, becoming white displacement noise. We call the f^2 analog filter *De-Whitening filter*.

Practically, we use a single zero-pole analog filter with transfer function showed in Fig.(4.1) as our De-Whitening filter.

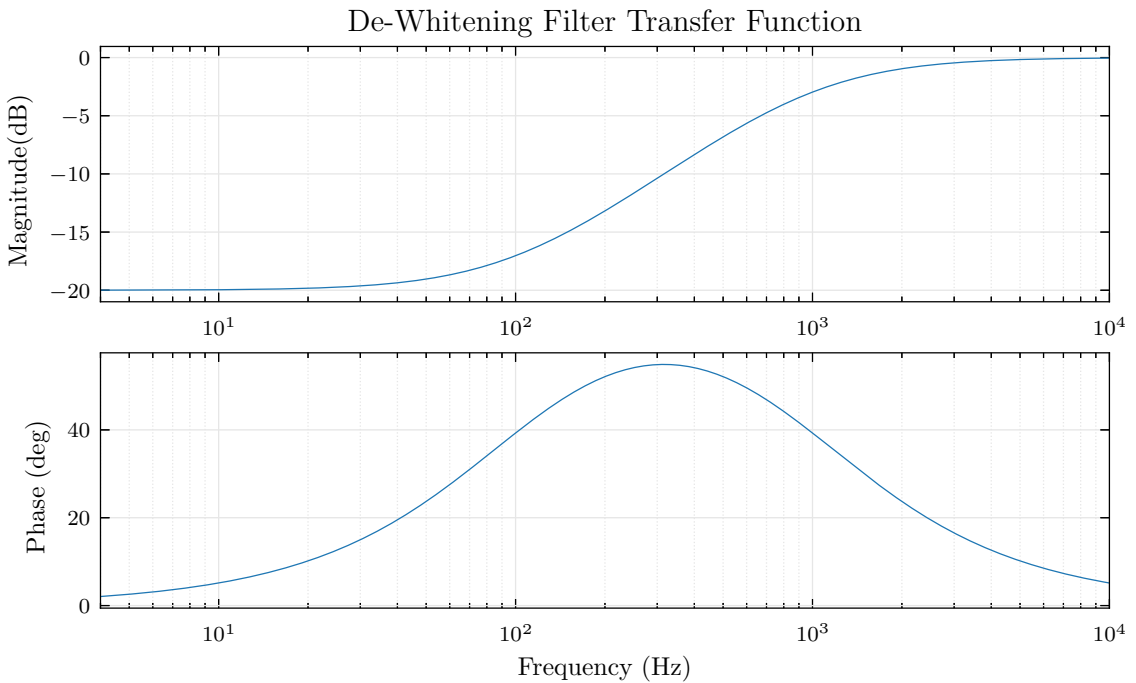


Figure 4.1: De-Whitening filter transfer function. This is the designed transfer function of De-Whitening filter. It has a pole at 1kHz and a zero at 100Hz.

4.2 Circuit Design

The main circuit design is described in Fig. 4.2. It converts a differential input signal into a single-ended one by an instrumentation amplifier. Then, the signal will pass through the De-Whitening stage, which attenuates the low-frequency signal while keeping the gain of the high-frequency signal unchanged. After that, we convert the filtered single-ended output to differential output, and send it to a downstream device.

The frequency dependent attenuation in the De-Whitening stage is realized by a single zero-pole analog filter. The pole and zero frequencies are determined by resistors and capacitors between A and B in Fig. 4.2. In order to reduce filter shape uncertainty caused by pole-zero frequency drifting, we use $0.01\mu\text{F}$ Mica capacitor (CD30FD103FO3F made by Cornell Dubilier Electronics), whose capacitance tolerance is within 1% and capacitance drift is within $\pm(0.05\% + 0.1\text{pF})$.

The transfer function of this circuit is

$$\text{DewTF} = \underbrace{\frac{Z_A}{Z_A + Z_B}}_{\substack{\text{pole-zero stage}}} \times \underbrace{2}_{\substack{\text{Single to Differential}}} \quad (4.1)$$

where

$$A//B \equiv \frac{1}{\frac{1}{A} + \frac{1}{B}} \quad (4.2)$$

$$Z_B = (R_3 + \frac{1}{i\omega C_2}) // R_b \quad (4.3)$$

$$Z_A = (R_4 + \frac{1}{i\omega C_1}) // R_a \quad (4.4)$$

When $R_3 = R_4 = a$, $C_1 = C_2 = C$, Eq. (4.1) will reduce to

$$\text{DewTF} = 2 \left(\frac{1 + i\omega C(a + R_b)}{1 + \frac{R_b}{R_a} + i\omega C(2R_b + a(1 + \frac{R_b}{R_a}))} \right) \quad (4.5)$$

Practically, we chose $a = 100\Omega \ll R_a = 8.34(88)\text{k}\Omega < R_b = 159.(3)\text{k}\Omega$ due to the availability of resistors in the market. Then, the DC gain is

$$\text{DewTF} |_{\omega=0} = \frac{2}{1 + \frac{R_b}{R_a}} = 0.0996 \quad (4.6)$$

It is about a factor of ten suppression of low-frequency signals while gains of high-frequency signals are kept unity. The pole and zero frequencies of such circuit are

$$\text{Zero} = \frac{1}{2\pi C(a + R_a)} = 99.8\text{Hz} \quad (4.7)$$

$$\text{Pole} = \frac{1}{2\pi C(a + 2\frac{R_a R_b}{R_a + R_b})} = 996.8\text{Hz} \quad (4.8)$$

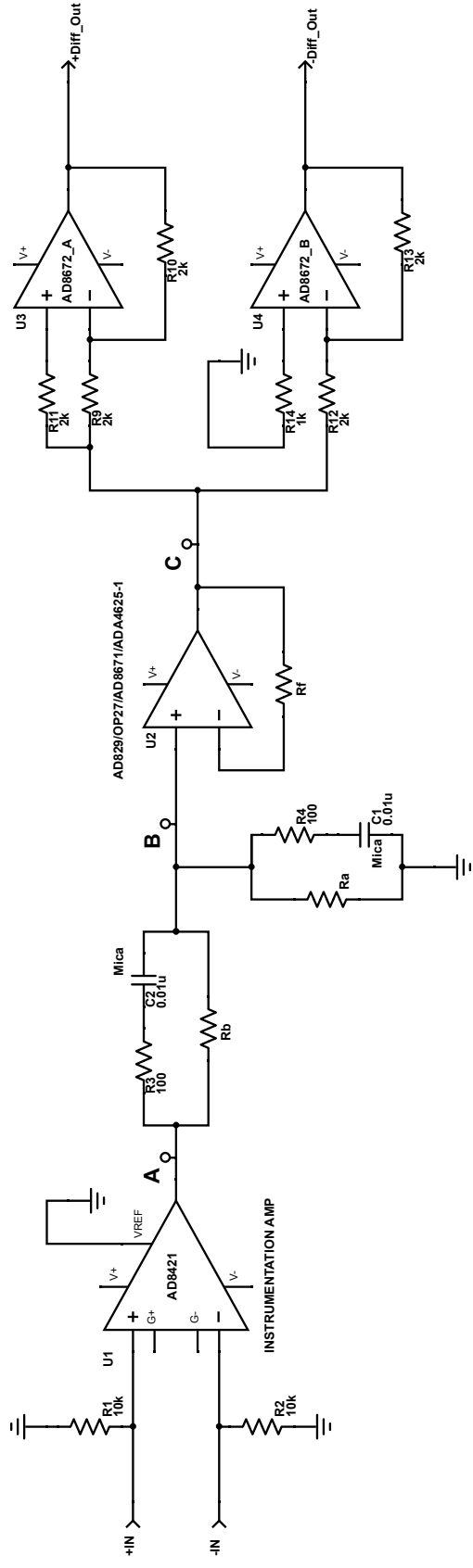


Figure 4.2: De-Whitening filter circuit. There are three points labeled as A, B, and C in the diagram. Before A, a differential input signal provided by Digital System will be converted into a single-ended signal by an instrumentation amplifier AD8421. After that, a passive pole-zero stage between A and B defines the dominate transfer function of the De-Whitening filter. Then we put a voltage follower between B and C as a buffer to keep passive filter response. Finally, we convert the signal back to a differential output to match the downstream device input.

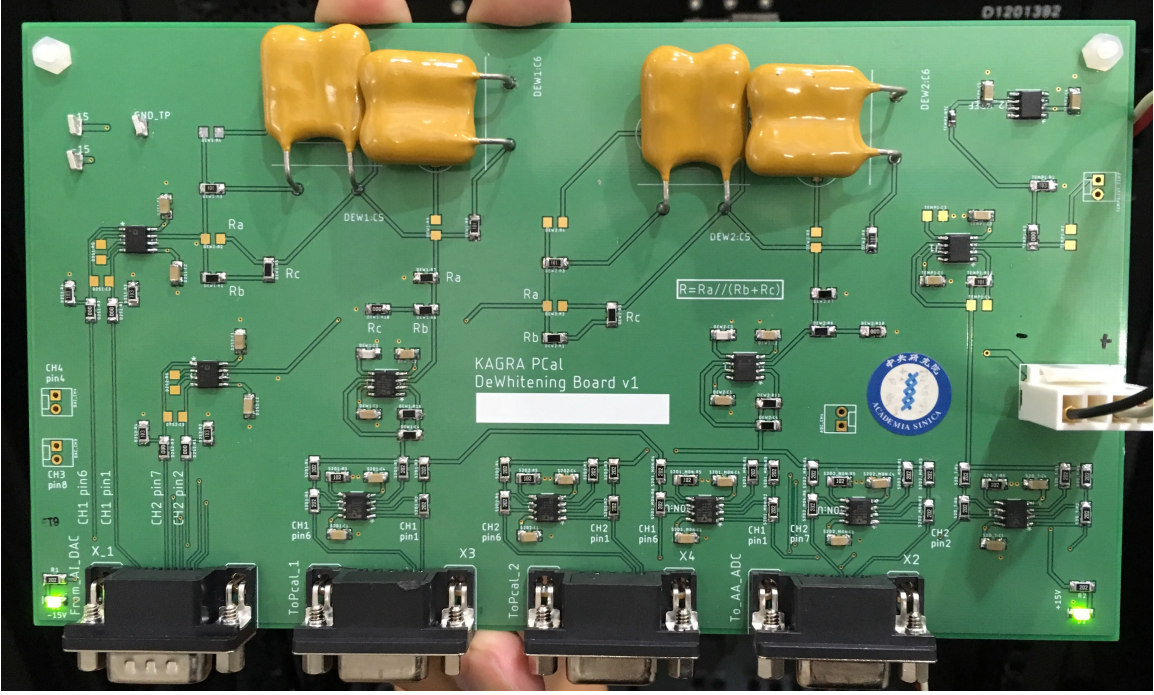


Figure 4.3: De-Whitening filter board. It's a 1.6mm FR-4 printed circuit board manufactured by SPEEDY Circuits Co., Ltd. The layout of this board is done with EAGLE, an EDA software. Four large yellow capacitors are Mica capacitors for the pole-zero stage. At KAGRA site, we installed it into a 1U chassis powered by a DC power supply with a LM2941/LM2991 voltage regulation circuit designed by LIGO.

4.3 Fidelity of Injection Signals

The fidelity of injected signals is the fundamental requirement of hardware injection test. One can estimate the distortion of the injected waveforms by measuring the transfer function between an excitation port in the software and the PCal laser intensity. After measuring such transfer function, we can create an inverse De-Whitening digital filter in software side to compensate for our analog De-Whitening filter. The combination allows us to suppress low-frequency noise from DAC while the transfer function for signal is kept unity.

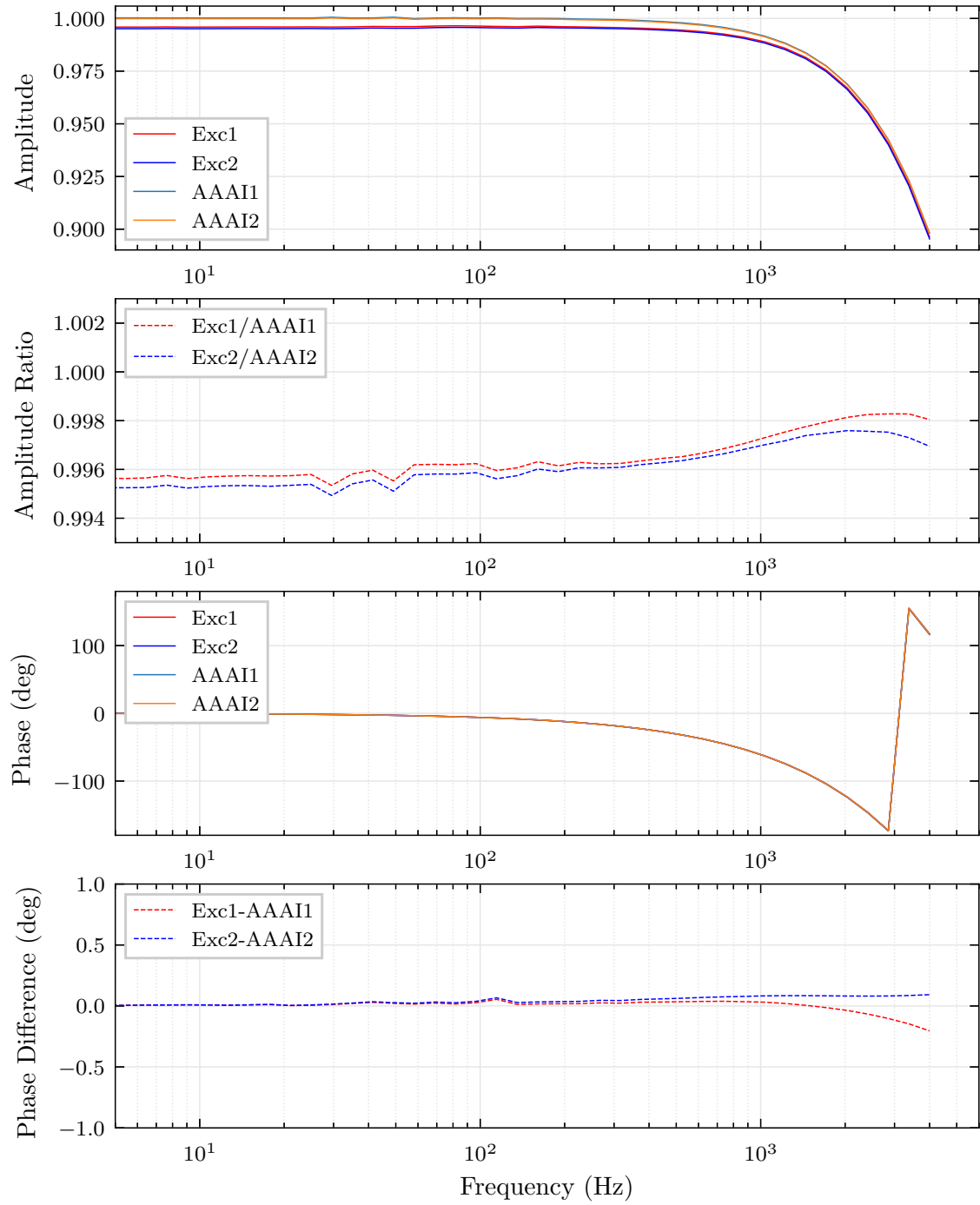


Figure 4.4: Transfer function of De-Whitening Filter with Digital Inverse Filter. The transfer function is measured in KEK cryogenic center with KAGRA standalone digital system and 64kHz slave model.

4.4 Noise Reduction Performance

We have tested the noise reduction performance of our De-Whitening Filter in KAGRA X-END. The noise is measured by the KAGRA Digital System with a third order whitening filter, which can amplify the signal above 10Hz for about 60dB. Exactly speaking, it has a third order zero at 10Hz and a third order pole at 1Hz in its amplification circuit.

The experimental setup is depicted in Fig. 4.5 and Fig. 4.6.

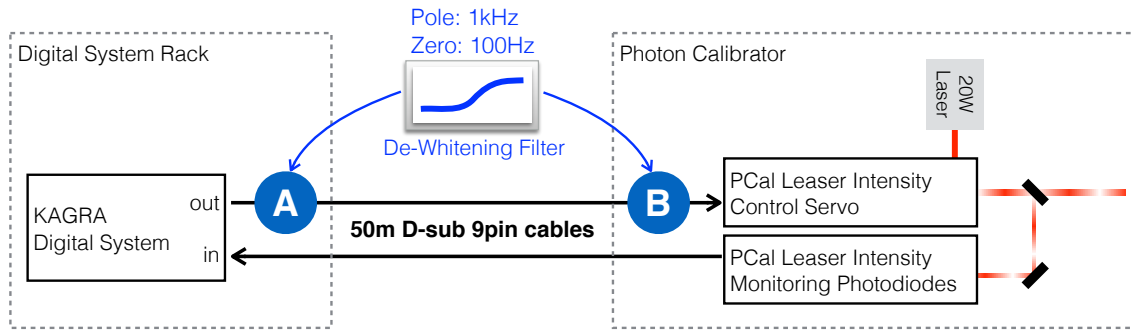


Figure 4.5: In order to reduce the noise coming from the digital system, the De-Whitening filter can be installed at either place A or B.

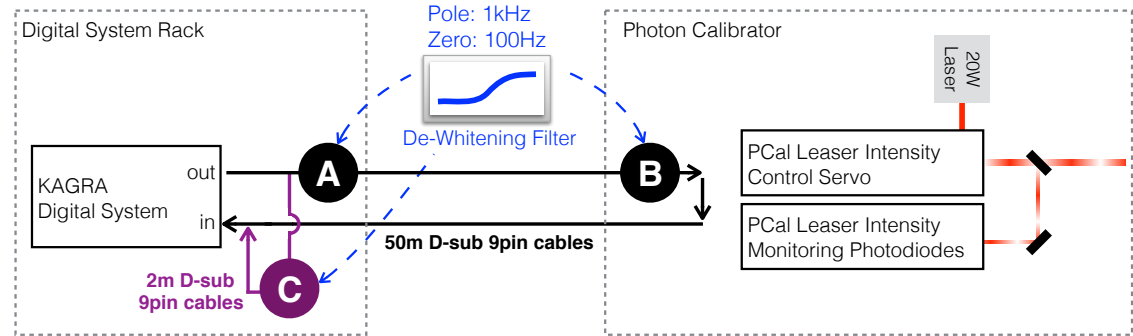


Figure 4.6: For our reference, we also measured the noise from the digital system without passing through the control loop of PCal. Place C means we connect De-Whitening filter in digital system rack with 2m cable only in order to investigate the influence from 50m cable.

The acronym used in legends in measurement plots are explained in Table 4.1.

Label in legend	Description
AI	Anti-Alias Chassis with Whitening Filter (as a preamplifier)
AA	Anti-Image Chassis
DEW	De-Whitening Filter

Table 4.1: Acronym of devices in noise measurement plots

4.4.1 Noise Measurement without PCal System

As described in Fig.(4.6), we have compared the noise from digital control system through different cable length with and without De-Whitening filter.

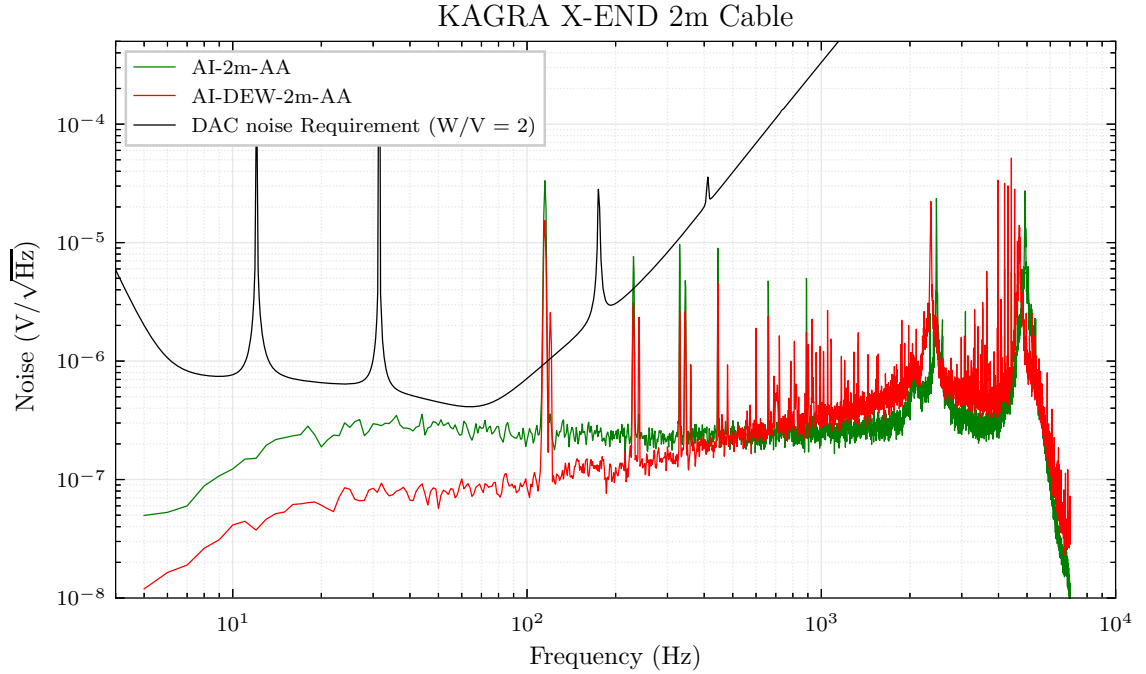


Figure 4.7: De-Whitening filter noise with short (2m) cable. The green line is the noise without De-Whitening filter, while the red one is the noise with De-Whitening filter.

Fig.(4.7) is the noise measurement result with 2m signal cable as described in Fig.(4.6). The low-frequency noise is suppressed by De-Whitening circuit. However, the amount of suppressing is not 20dB. It is possible that we hit another noise floor at $10^{-7}\text{V}/\sqrt{\text{Hz}}$ due to the internal noise of the De-Whitening filter circuit. Below 10Hz, the measured noise is less than actual noise since we used the a customized high-pass filter, i.e. a Whitening Chassis, to prevent the saturation of measurement instrument by any small DC offset. Same effect is exist in all noise measurement results in this thesis since we adopted same measuring scheme.

In the end station of KAGRA, unfortunately, the digital system rack is placed near the ETM, which is 36m far away from PCal system. Therefore, the practical control

signal is carried by 50m D-sub cables as illustrated in Fig.(4.5) at this moment. As a result, we tried to perform the same noise measurement with 50m cables. The result is in Fig.(4.8).

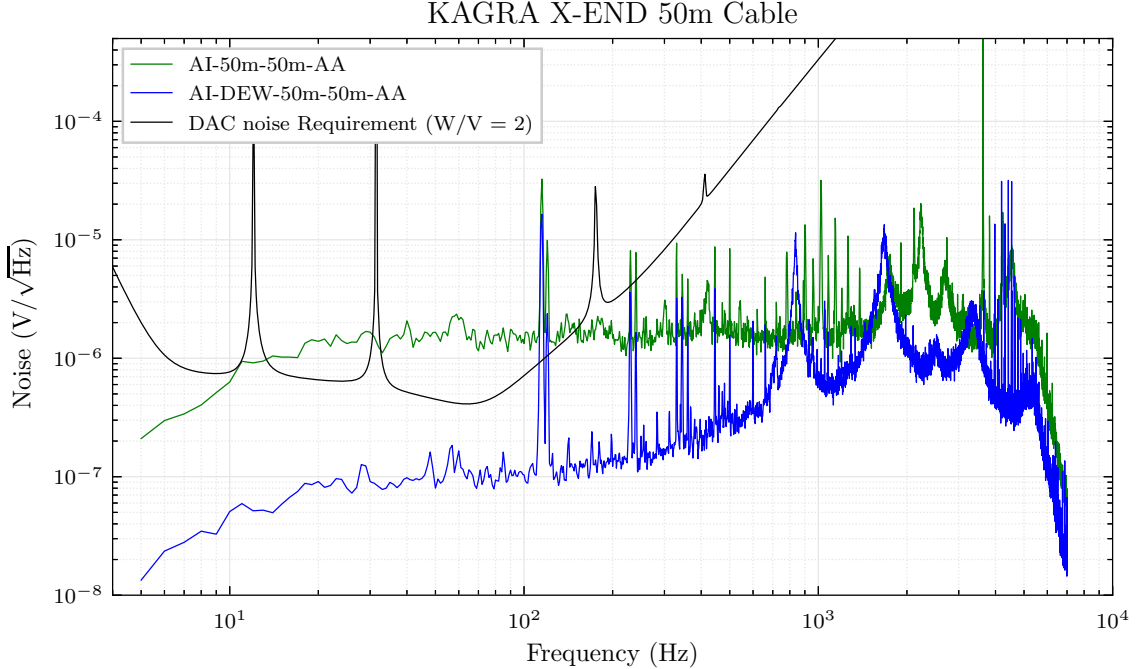


Figure 4.8: De-Whitening filter noise with long (50m) cable.

With 50m cable, the unsuppressed noise (green line in Fig.(4.8)) is larger than 2m one (green line in Fig.(4.7)) due to unknown reason. However, the 20dB suppression capability can be verified in Fig.(4.8).

In Fig.(4.9), we overplot the suppressed noise by De-Whitening filter in 2m and 50m cable case. Although the 50m case has some noise excess around kHz regime, their low-frequency noise performance do not have significant difference. This result imply that the $10^{-7}V/\sqrt{Hz}$ noise floor can really come from De-Whitening circuit itself. In the future, we may come back into this issue when we have more strict noise requirement that will be the case if we decide to use higher power Pcal laser or have better interferometer sensitivity.

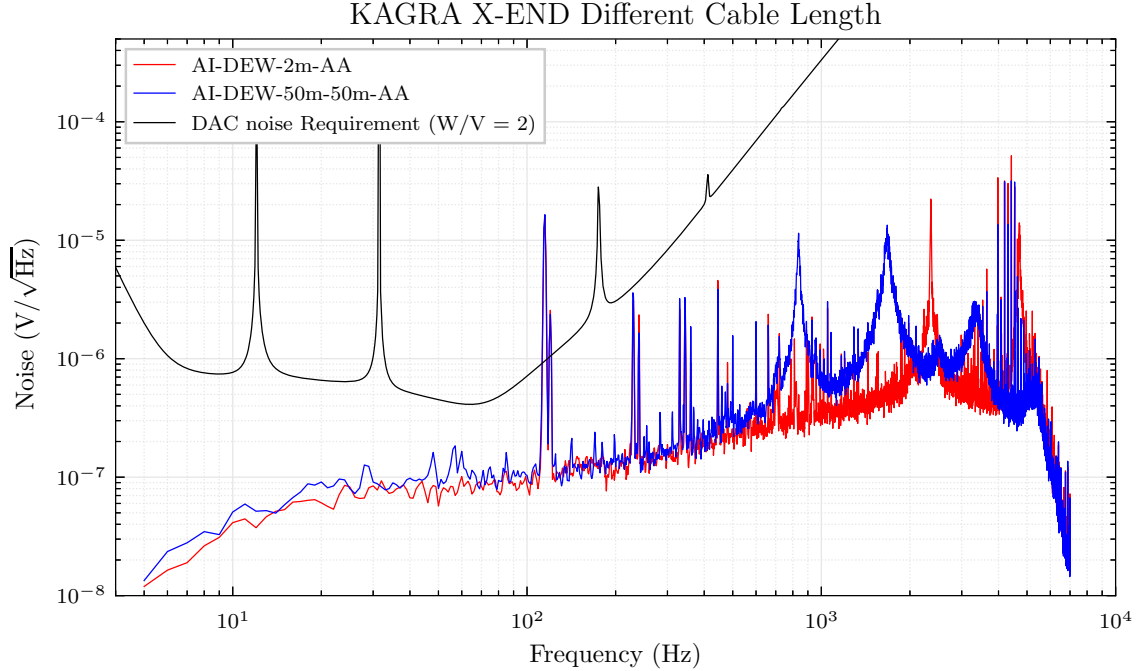


Figure 4.9: De-Whitening filter noise with different cable length.

Since we observed that the unattenuated noise floor in 50m cable case is larger, we suspect that some environmental noises are picked up by the cable. We tried to install our De-Whitening filter in either place A or B in Fig.4.6 and the result is in Fig.4.10. Originally, we thought if the extra noise is picked up by the cable, it should be attenuated when we install the De-Whitening filter at place B. However, the red line in Fig.4.10 shows that if we put our De-Whitening filter at place B, the measured noise is actually higher than the one without De-Whitening filter.

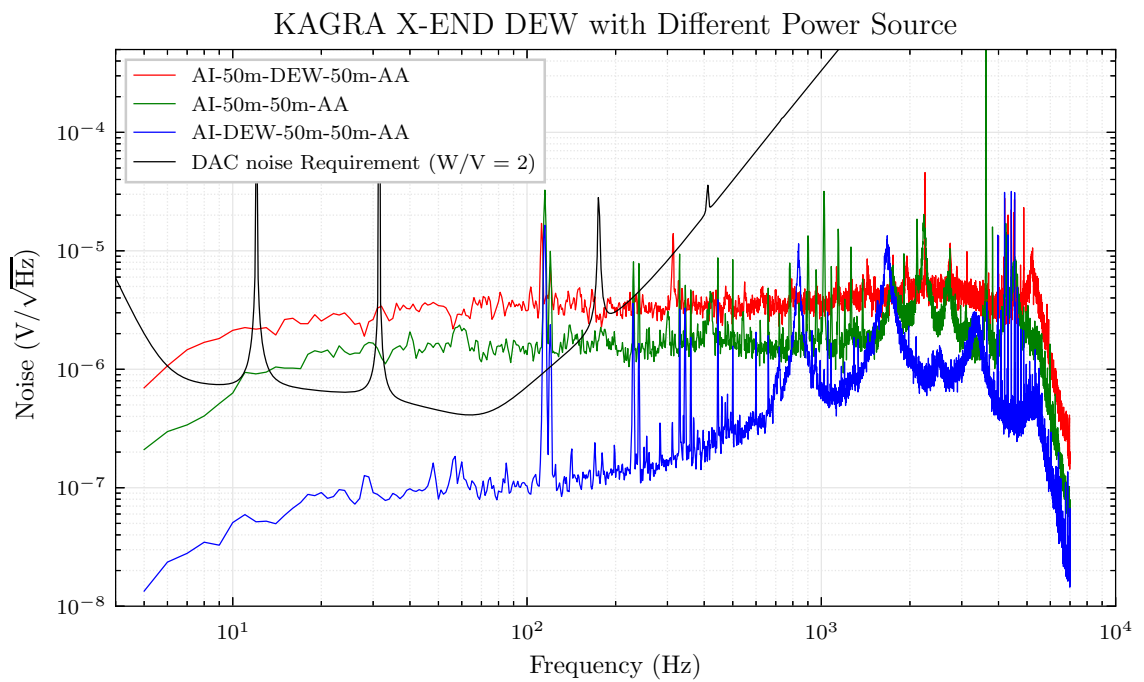


Figure 4.10: Noise measurement when the De-Whitening filter is installed at different location.

4.4.2 Noise Measurement with PCal System

Now, it is the time to connect the Digital System and the De-Whitening filter to our Photon Calibrator. The practical setup is illustrated in Fig. 4.5.

First, we try to understand how much low-frequency noise could be suppressed by De-Whitening filter. However, Fig. 4.11 indicates that something bad happened. Even though in the case with the De-Whitening, the noise decreases from blue line to red line in Fig. 4.11, it dose not follow the transfer function of De-Whitening filter, which can only suppress low-frequency noise.

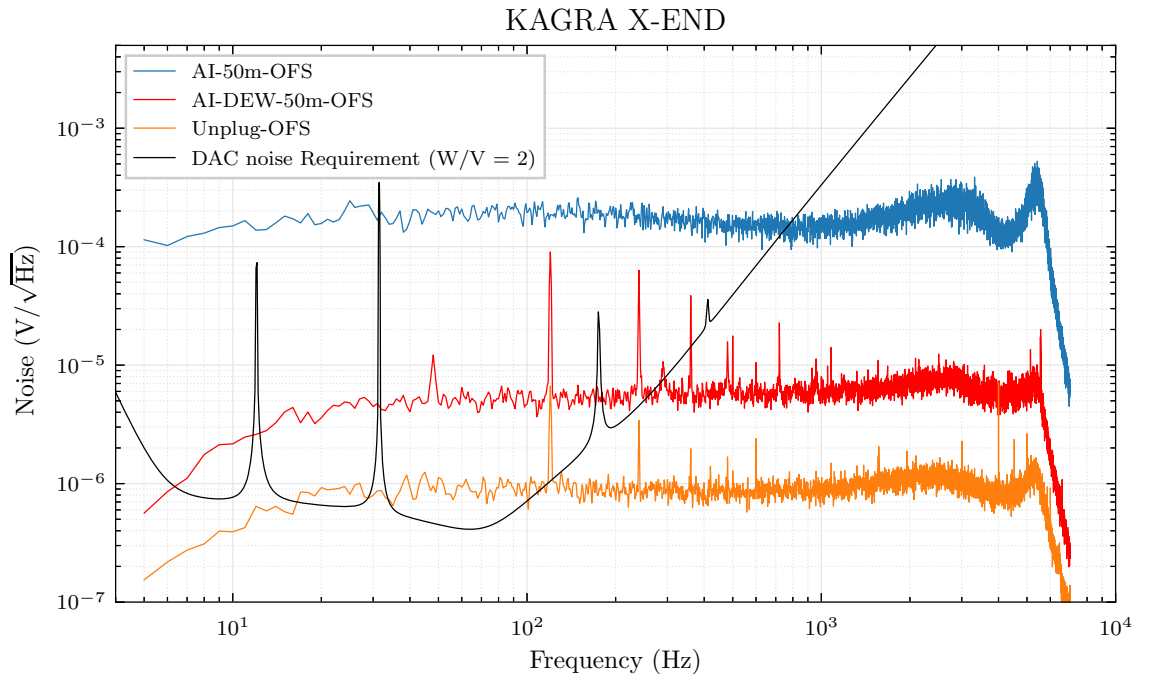


Figure 4.11: Noise measurement with PCal. These noises can be considered as laser intensity noises since we are measuring photodiode readout as depicted in Fig. 4.5. The blue line is the case without De-Whitening filer, while the red line is the case when De-Whitening filer has been installed at place A in Fig. 4.5. The orange line is measured when we disconnect our signal cable from the Laser Intensity Control Servo input port.

On the other hand, the orange line is the nosies when we disconnect the digital system output from our PCal. It is lower than either one of connected cases (blue and red). Besides, it is also higher than the noise that are plotted in Fig.(4.9), which is supposed to be the noise that be sent to PCal from the output of De-Whitening

filter. It reveals that the blue and the red lines in Fig. 4.11 is actually popped out just when we connect the digital system and our PCal together. We doubt that we may create the infamous grounding loop unintentionally. As a trial, we tried two different measurements. First, we put our De-Whitening filter in either place A or B in Fig. 4.5 and the result is in Fig. 4.12. Second, we supplied our Pcal from the DC power source located at digital system rack, which is shared with De-Whitening filter and other analog chassis of the digital system, including Anti-Image, Anti-Alias, and Whiting chassis. The result is given in Fig. 4.13.

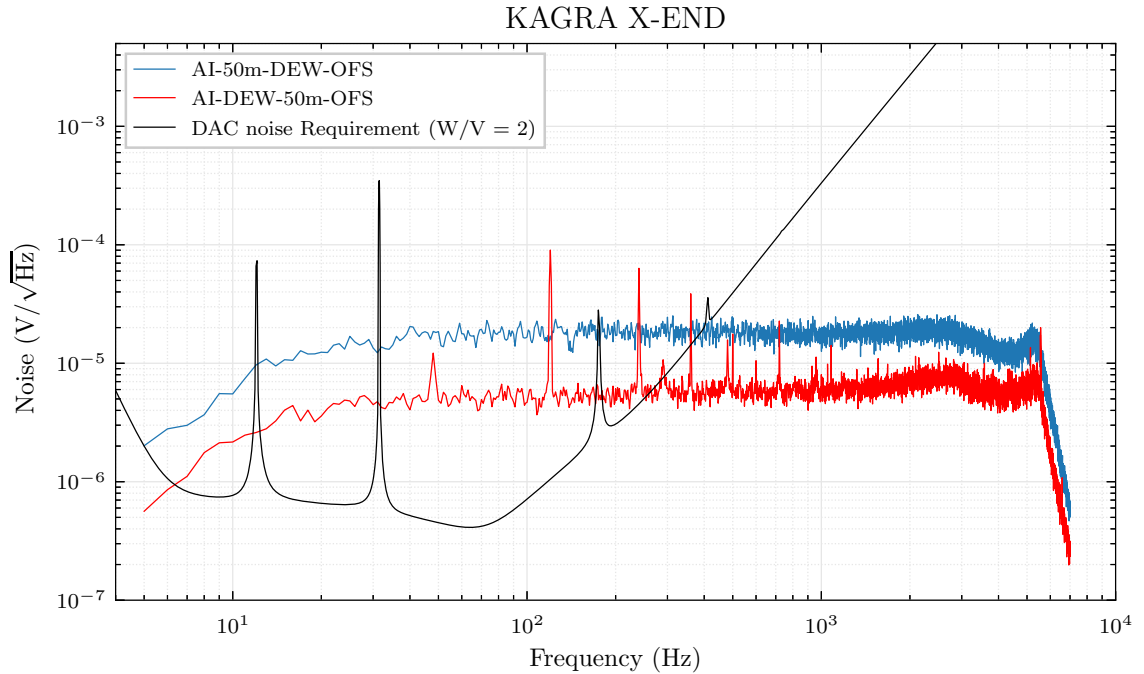


Figure 4.12: The red line and the blue line are measured when De-whitening is located at Place A and Place B in Fig. 4.5 respectively.

Fig. 4.12 shows that if we install our De-Whitening filter at Place B in Fig. 4.5, we got a higher noise floor. The similar effect has been observed in Fig. 4.10.

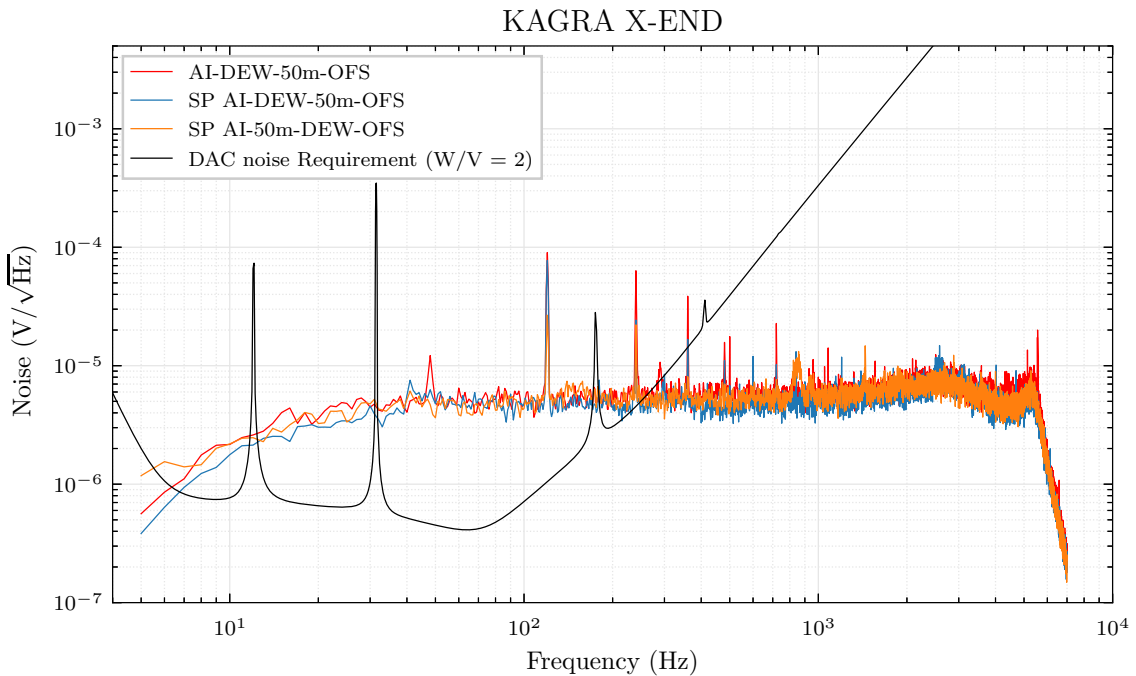


Figure 4.13: Lines labeled with “SP” were measured when we supplied digital system, De-Whitening filter and PCal with Same Power source located in digital system rack.

When we supply our PCal with the shared power source in the digital system rack, the noise floors become independent of the location of De-Whitening filter as you can observe in Fig. 4.13. They are also coincident with the red line in the plot. Among measurements we have tried, whenever the De-Whitening filter is supplied by the same power source as Anti-Image chassis, which is the upstream device of De-Whitening filter, the noise floor we get becomes the same as the red line in Fig. 4.13.

Chapter 5

Validation of Injection Channel

Without loss of generality, We injected several binary blackhole (BBH) signals into PCal to test the performance of our De-Whitening Filter. Unfortunately, at this moment, we couldn't find a compatible data-taking system with desired noise level and dynamical range to faithfully reconstruct or estimate the expect End-Test Mirror (ETM) displacement that caused by our Photon Calibrator. The reason is that the ADC we used has much larger noise than the DAC we used. To beat the ADC noise, although we can amplify the signal before feeding it into the ADC, as what we did for noise measurement in last chapter, some part of injected waveform can easily saturate our ADC. Therefore, the results showed in this chapter should be treated as a demonstration of injecting simulated GW waveforms to PCal. The result should not be used for estimating noise performance.

In Fig. 5.1, we have chosen three different binary blackholes (BBH) coalescence waveform templates. All of them are equal-mass BBH system whose individual masses are 10, 20, and 30 solar mass correspondingly. They could have different portion of their signal that fit into the most sensitive frequency of the KAGRA detector. This can be helpful for some purposes, e.g. testing General Relativity [23]. If we can inject these signals into our main interferometer in the future, we could have a chance to

test the response of KAGRA to these injections, thereby contributing to related BBH analysis works. The distance from the source to the detector is set to be 100 Mpc, which is a relative optimistic choice.

The injected waveform template is originally generated by *IMRPhenomD*¹ code in *LALSuite*². We selected a polarization mode of the strain waveform and translated it into the expected differential arm length change of 3 km KAGRA arms. Then, we calculated the required PCal power modulation according to Eq. (2.2). Next, the signal was injected through the *multiawgstream*³ program to the PCal control realtime model, in which the digital inverse De-Whitening filter has been implemented. Finally the output from Digital System was fed into our De-Whitening filter, and sent to the excitation port of our PCal, thereby modulating the intensity of PCal output laser beams.

One thing I have to mention here is that when we perform the injection test, the absolute Laser Intensity of our PCal is not calibrated accurately yet. In the future we have to calibrate it by a customized power meter, i.e. the Working Standard KAGRA (WSK), which is an integrating sphere followed by a photodiode and could be used for cross checking the absolute intensity of each PCal lasers across the worldwide gravitational wave detector network and also the laser power standard in some institutes, e.g. NIST⁴.

¹IMRPhenomD is a phenomenological binary blackhole coalescence waveform generating method including both Inspiral, Merger, and Ringdown phase.

²LALSuite is the LIGO Scientific Collaboration Algorithm Library Suite.

³multiawgstream is a program design by LIGO for injecting time series data into a specified channel in realtime models. In our case, the signal will be sent to PCal control model and result in corresponding DAC output for PCal laser intensity control.

⁴NIST is the National Institute of Standards and Technology in the United States.

Label in legend	Description
template	The data in the injected signal file.
50m	Without PCal, only through 50m+50m cables as a test of Digital System.
DEW50m	Same as the 50m but includes De-Whitening Filter and its digital inverse.
DEW50mCL	With De-Whitening filter, its digital inverse, and PCal.
DEW50mCL2	Same as DEW50mCL, a second time test with the identical setup.

Table 5.1: Explanation of legends in the injection result

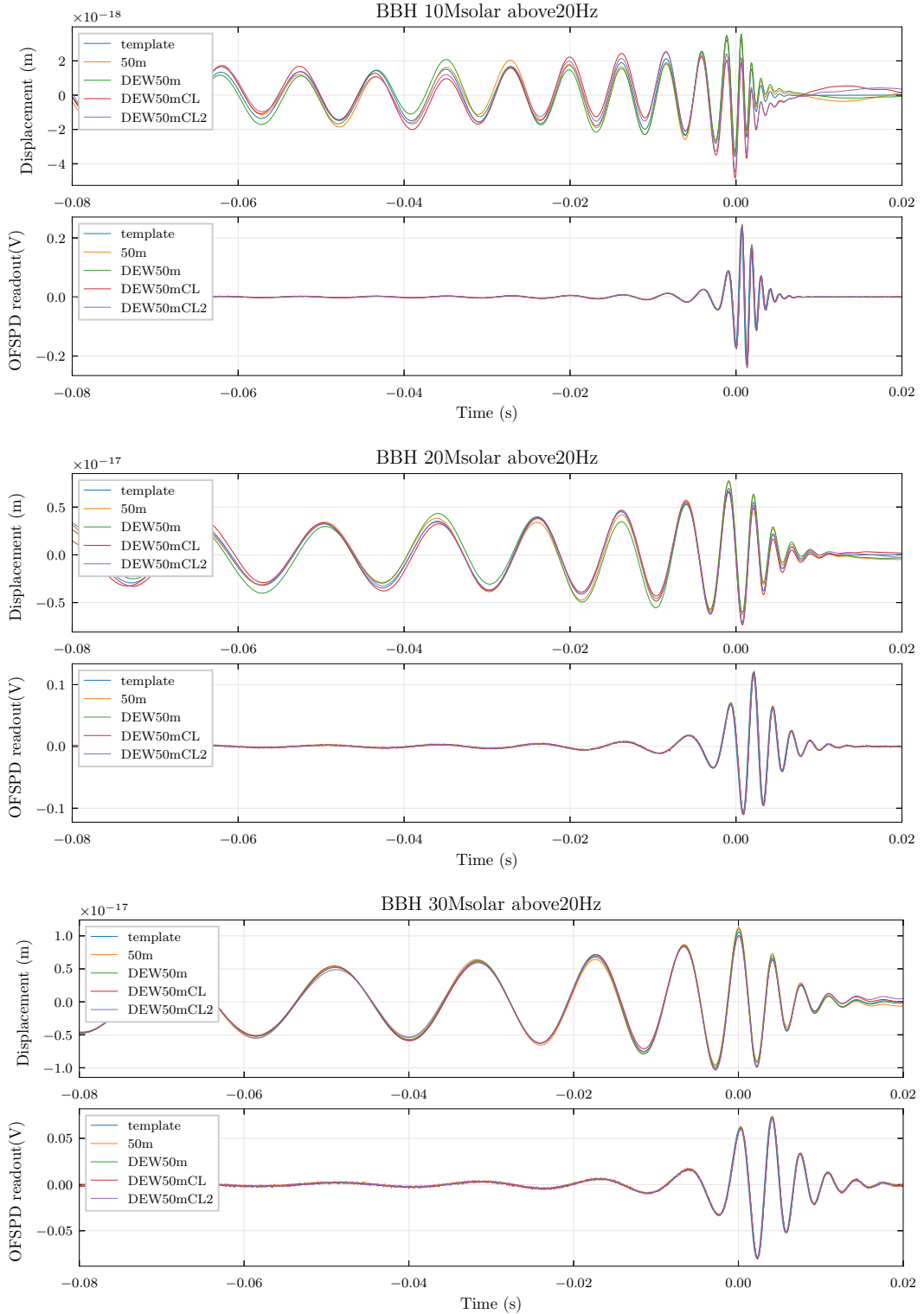


Figure 5.1: Injected Binary Blackhole Merger Signals. The lower panel of each plots is the electrical readout from a photodiode (OFSPD) in the PCal. It is proportional to the intensity of the PCal laser beam. The upper panel of each plots shows the theoretically estimated ETM displacement by applying $1/\omega^2$ force-to-length transfer function to the observed laser intensity. The meaning of the legend is explained in Table 5.1

Chapter 6

Discussion and Future Works

Although the De-Whitening Filter can attenuate low frequency noise and effectively increase low frequency signal resolution, it limits the maximum excitation signal that can be sent to Photon Calibrator. This is one of intrinsic disadvantages of the De-Whitening filter. In Fig.6.1 we estimated how much dynamical range will be sacrificed.

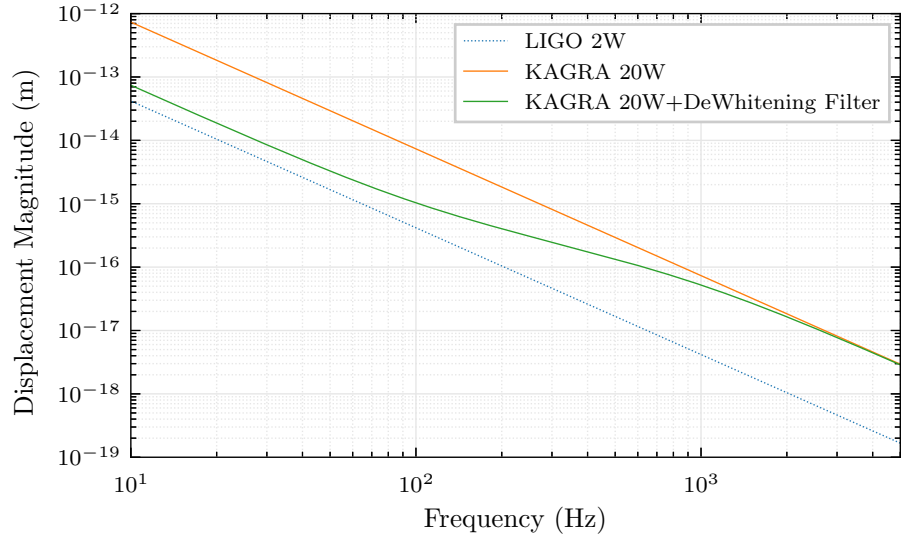


Figure 6.1: Maximum Injection Capability. This is the maximum, assuming 100 percent optical efficiency, displacement of ETM could be generated by Photon Calibrator. It proportional to $1/f^2$ due to the force-to-displacement transfer function of suspended ETM. The green line indicate the maximum laser intensity modulation amplitude that is attenuated by De-Whitening filter.

For the quantization noise from DAC, one can adopt the so-called *Noise Shaping* algorithm [24] to move the low frequency noise to the higher frequency regime, which will be removed by an anti-image filter before it comes into our PCal. Although it cannot increase the low frequency signal resolution that limited by DAC bit-depth, it dose not compromise maximum signal amplitude. As long as it is an approach independent approach to decrease the noise, we can apply it and De-Whitening filter at the same time if necessary.

On the other hand, naively, the noise problem can be solved by using a higher bit-depth DAC card. However, DACs with bit-depths higher than 16bits typically suffer from another noise source due to its *Integral Nonlinearity* (ref). Unless we dedicate significant resources into developing such high precision DAC chip and its auxiliary circuit, it might be challenging to find a satisfying commercial product at this moment.

During the experiments, we found that carrying analog signals on 50m long D-sub cables may be problematic because we have such strict noise requirement. Installation of an extra digital control system near our PCal is favored.

We have successfully modulate PCal laser intensity according to several binary blak hole coalescence waveform templates. Once the main KAGRA interferometer start working, we can verify whether the ETM displacement has been generated as we expected. At the same time, will have ability to crosscheck the response of main interferometer, which is the main goal of hardware injection test.

Bibliography

- [1] C. Biwer et al. Validating gravitational-wave detections: The Advanced LIGO hardware injection system. *Phys. Rev. D*, 95:062002, Mar 2017. doi: 10.1103/PhysRevD.95.062002. URL <https://link.aps.org/doi/10.1103/PhysRevD.95.062002>.
- [2] A Einstein. Grundgedanken und Methoden der Relativitätstheorie, in ihrer Entwicklung dargestellt. Fundamental Ideas and Methods of the Theory of Relativity, Presented in Their Development, after 22 Jan 1920. 1920. URL <https://einsteinpapers.press.princeton.edu/vol7-trans/129>.
- [3] Daniel Kennefick. Einstein versus the physical review. *Physics Today*, 58(9):43–48, 2005. doi: 10.1063/1.2117822. URL <https://doi.org/10.1063/1.2117822>.
- [4] A. Einstein and N. Rosen. On gravitational waves. *Journal of the Franklin Institute*, 223(1):43 – 54, 1937. ISSN 0016-0032. doi: [https://doi.org/10.1016/S0016-0032\(37\)90583-0](https://doi.org/10.1016/S0016-0032(37)90583-0). URL <http://www.sciencedirect.com/science/article/pii/S0016003237905830>.
- [5] R. A. Hulse and J. H. Taylor. Discovery of a pulsar in a binary system. *ApJ*, 195:L51–L53, January 1975. doi: 10.1086/181708.
- [6] J. H. Taylor and J. M. Weisberg. A new test of general relativity - Gravitational radiation and the binary pulsar PSR 1913+16. *ApJ*, 253:908–920, February 1982. doi: 10.1086/159690.
- [7] Joseph H. Taylor. Binary pulsars and relativistic gravity. *Rev. Mod. Phys.*, 66: 711–719, Jul 1994. doi: 10.1103/RevModPhys.66.711. URL <https://link.aps.org/doi/10.1103/RevModPhys.66.711>.
- [8] B. P. Abbott et al. Observation of gravitational waves from a binary black hole merger. *Phys. Rev. Lett.*, 116:061102, Feb 2016. doi: 10.1103/PhysRevLett.116.061102. URL <https://link.aps.org/doi/10.1103/PhysRevLett.116.061102>.
- [9] M. Maggiore and Oxford University Press. *Gravitational Waves: Volume 1: Theory and Experiments*. Gravitational Waves. OUP Oxford, 2008. ISBN 9780198570745. URL <https://books.google.com.tw/books?id=AqVpQgAACAAJ>.

- [10] Malik Rakhmanov. Response of test masses to gravitational waves in the local lorentz gauge. *Phys. Rev. D*, 71:084003, Apr 2005. doi: 10.1103/PhysRevD.71.084003. URL <https://link.aps.org/doi/10.1103/PhysRevD.71.084003>.
- [11] Evan D. Hall, Craig Cahillane, Kiwamu Izumi, Rory J. E. Smith, and Rana X. Adhikari. Systematic calibration error requirements for gravitational-wave detectors via the Cramér-Rao bound. 2017.
- [12] A D Viets, M Wade, A L Urban, S Kandhasamy, J Betzwieser, Duncan A Brown, J Burguet-Castell, C Cahillane, E Goetz, K Izumi, S Karki, J S Kissel, G Mendell, R L Savage, X Siemens, D Tuyenbayev, and A J Weinstein. Reconstructing the calibrated strain signal in the advanced ligo detectors. *Classical and Quantum Gravity*, 35(9):095015, 2018. URL <http://stacks.iop.org/0264-9381/35/i=9/a=095015>.
- [13] D Tuyenbayev, S Karki, J Betzwieser, C Cahillane, E Goetz, K Izumi, S Kandhasamy, J S Kissel, G Mendell, M Wade, A J Weinstein, and R L Savage. Improving ligo calibration accuracy by tracking and compensating for slow temporal variations. *Classical and Quantum Gravity*, 34(1):015002, 2017. URL <http://stacks.iop.org/0264-9381/34/i=1/a=015002>.
- [14] DA Clubley, GP Newton, KD Skeldon, and J Hough. Calibration of the glasgow 10 m prototype laser interferometric gravitational wave detector using photon pressure. *Physics Letters A*, 283(1-2):85–88, 2001.
- [15] H P Daveloza, M Afrin Badhan, M Diaz, K Kawabe, P N Konverski, M Landry, and R L Savage. Controlling calibration errors in gravitational-wave detectors by precise location of calibration forces. *Journal of Physics: Conference Series*, 363(1):012007, 2012. URL <http://stacks.iop.org/1742-6596/363/i=1/a=012007>.
- [16] S. Karki et al. The advanced ligo photon calibrators. *Rev. Sci. Instrum.*, 87: 114503, 2016.
- [17] Rolf Bork. Advligo cds design overview. *LIGO Document Control Center*, (Report No. T0900612), 2010. URL <https://dcc.ligo.org/LIGO-T0900612/public>.
- [18] J. Heefner R. Abbott. Advanced ligo anti-aliasing and anti-image filter function. *LIGO Document Control Center*, (Report No. T070038), 2007. URL <https://dcc.ligo.org/LIGO-T070038/public>.
- [19] R. Bork and A. Ivanov. Advligo cds realtime sequencer software. *LIGO Document Control Center*, (Report No. T0900607), 2012. URL <https://dcc.ligo.org/LIGO-T0900607/public>.
- [20] R. Bork. Real-time code generator (rcg) software component overview. *LIGO Document Control Center*, (Report No. T1200291), 2012. URL <https://dcc.ligo.org/LIGO-T1200291/public>.

- [21] A. Ivanov R. Bork, M. Aronsson. Advligo cds realtime code generator (rcg) application developer's guide. *LIGO Document Control Center*, (Report No. T080135), 2013. URL <https://dcc.ligo.org/LIGO-T080135/public>.
- [22] Y. Enomoto et al. Latest estimated sensitivity of kagra (v201708) *approved*. *JGW Document Database*, (Report No. JGW-T1707038-v7), 2017. URL <https://gwdoc.icrr.u-tokyo.ac.jp/cgi-bin/DocDB>ShowDocument?docid=7038>.
- [23] B. P. Abbott et al. Binary black hole mergers in the first advanced ligo observing run. *Phys. Rev. X*, 6:041015, Oct 2016. doi: 10.1103/PhysRevX.6.041015. URL <https://link.aps.org/doi/10.1103/PhysRevX.6.041015>.
- [24] Ayush Pandey, Christopher Wipf, Rana Adhikari, and Jameson Graef Rollins. Quantization noise in advanced ligo digital control systems. *LIGO Document Control Center*, (Report No. T1500351), 2015. URL <https://dcc.ligo.org/LIGO-T1500351/public>.